applied sciences

MDPI

Article

Design of Road-Side Barriers to Mitigate Air Pollution near Roads

Jose I. Huertas [1,*], Javier E. Aguirre [1], Omar D. Lopez Mejia [2] and Cristian H. Lopez [2]

[1] Energy and Climate Change Research Group, School of Engineering and Science, Tecnologico de Monterrey, Monterrey 64849, Mexico; A00814954@itesm.mx
[2] Computational Mechanics Research Group, Department of Mechanical Engineering, Universidad de los Andes, Bogotá 111711, Colombia; od.lopez20@uniandes.edu.co (O.D.L.M.); ch.lopez@uniandes.edu.co (C.H.L.)
* Correspondence: jhuertas@itesm.mx

Abstract: The effects of using solid barriers on the dispersion of air pollutants emitted from the traffic of vehicles on roads located over flat areas were quantified, aiming to identify the geometry that maximizes the mitigation effect of air pollution near the road at the lowest barrier cost. Toward that end, a near road Computational Fluid Dynamics (NR-CFD) model that simulates the dispersion phenomena occurring in the near-surface atmosphere (<250 m high) in a small computational domain (<1 km long), via Computational Fluid Dynamics (CFD) was used. Results from the NR-CFD model were highly correlated ($R^2 > 0.96$) with the sulfur hexafluoride (SF_6) concentrations measured by the US-National Oceanic and Atmospheric Administration (US-NOAA) in 2008 downwind a line source emission, for the case of a 6m near road solid straight barrier and for the case without any barrier. Then, the effects of different geometries, sizes, and locations were considered. Results showed that, under all barrier configurations, the normalized pollutant concentrations downwind the barrier are highly correlated ($R^2 > 0.86$) to the concentrations observed without barrier. The best cost-effective configuration was observed with a quarter-ellipse barrier geometry with a height equivalent to 15% of the road width and located at the road edge, where the pollutant concentrations were 76% lower than the ones observed without any barrier.

Keywords: CFD; near road emissions; solid barriers; gas-phase pollutants; air pollution mitigation

Citation: Huertas, J.I.; Aguirre, J.E.; Lopez Mejia, O.D.; Lopez, C.H. Design of Road-Side Barriers to Mitigate Air Pollution near Roads. *Appl. Sci.* **2021**, *11*, 2391. https://doi.org/10.3390/app11052391

Academic Editor: José Carlos Magalhães Pires

Received: 15 February 2021
Accepted: 3 March 2021
Published: 8 March 2021

1. Introduction

In urban centers, vehicles are the main source of fine (d < 10 μm) and ultrafine (d < 100 nm) particles, black carbon, carbon monoxide (CO), and nitrogen oxides (NO_x) [1,2]. These air pollutants cause respiratory and cardiovascular problems, chronic diseases, and early mortality in the people exposed to these pollutants [3,4]. Studies have shown that within urban regions, pedestrians and people living near roads (<500 m) are exposed to the highest concentration levels of these pollutants [5].

Therefore, there is an urgent need for the design of countermeasures to reduce pollutant concentration near roads. This need is an example of a more general problem, which is the design of countermeasures to reduce pollutant concentration near area sources of pollutants located on flat regions, such as, paved and unpaved roads; uncovered areas exposed to the wind action, such as desertic areas, and particulate materials stored at open atmosphere (carbon piles as an example); gaseous leaks from pipes (natural gas pipes as an example); gases evaporated from pools exposed to open atmosphere (hydrocarbon spillages and sewer water as examples); and agro-industrial open burning.

Barriers have been widely used for near-road noise control. However, as shown in Table 1, it has been found that the use of natural or human-made barriers located on the roadsides has the potential of reducing those concentrations. Nevertheless, the improper design of those barriers could end up increasing those concentrations or moving the concentration peaks to some distance down downwind the road.

Table 1. Relevant studies of the last decade regarding the use of barriers for the dispersion of air pollutants.

Author(s)	Description	Year	CFD	Experimental Measurements	Geometry Variation	Cost Evaluation
Finn et al.	Tracer gas dispersion study with a straight noise barrier near roadway	2009	x	✓	x	x
Ning et al.	Impact of noise barriers on particle pollutants size distributions and concentrations near freeways	2010	x	✓	x	x
Hagler et al.	Use of tree stands and brick noise barriers for mitigation of roadside ultrafine particles	2012	x	✓	✓	x
Steffens et al.	Vegetation barrier model to mitigate roadside pollutant dispersion in terms of LAD	2012	✓	✓	x	x
Steffens et al.	Simulation of tracer gas dispersion under twelve different roadway configurations	2013	✓	✓	✓	x
Adair and Jaeger	Evaluation of solid barriers performance for the mitigation of air pollution with NOx	2014	✓	✓	✓	x
Busini et al.	Barrier shape effect on LNG dispersion due to pipe leaks	2014	✓	✓	✓ [1]	x
Schulte et al.	Semiempirical dispersion model of roadside barriers	2014	x	✓	✓	x
Jin Jeong	Roadside barrier impact on the dispersion of road air CO for several road configurations	2015	✓	✓	x	x
Morakinyo and Lam	PM dispersion and removal via natural barrier use	2015	✓	✓	✓	x
Baldauf et al.	Noise barriers for the mitigation of on-road and downwind pollutants (NOx, UFP)	2016	x	✓	x	x
Tong et al.	Effects of vegetative and solid barriers on the mitigation of particle matter pollutants	2016	✓	✓	✓	x
Gerdroodbary et al.	Mesh barrier use to mitigate ammonia dispersion near pipelines	2016	✓	✓	✓ [2]	x
Ranasinghe et al.	Vegetation and barrier combination effect on pollutant dispersion near roads	2019	x	✓	x	x
Wang and Wang	Effect of vehicle shape and barrier use on highway emission dispersion	2020	✓	✓	x	x
Reiminger et al.	Effect of wind speed and atmospheric stability on pollutant reduction rate due to barrier use	2020	✓	✓	x	x
Venkatram et al.	Pollutant dispersion near road-side barrier edges	2021	x	✓	x	x

[1] Barrier with a tilted upper section (45° and 63° from +y); [2] Mesh barrier variation: Number and size of holes in geometry.

Experimental studies: Several of the studies carried out related to barriers are experimental, and include solid and vegetative barriers [6]. One of the most well-known experimental studies is the one performed by the National Oceanic and Atmospheric Administration (NOAA) in Idaho Falls, USA [7] and reported by Finn et al. [5], where sulfur hexafluoride (SF_6) was dispersed into two different areas, one with a 54 m long and 6m high barrier and the other without any obstacle to the free flow. Results showed that in the presence of the barrier, the SF_6 concentration was reduced by 15–50%. Said study was reproduced inside a wind tunnel by Heist et al. [8] and obtained a concentration reduction of up to 85%. Hagler et al. [9] reported that the concentration of ultrafine particles in the presence of a 6m barrier is less than 50% just after the barrier compared to the base case without the barrier in major roadways in central North Carolina, USA. Schulte et al. [10] found that the pollutants concentration reduction downwind the barrier can increase with the height as a result of the turbulence induced by the presence of said barrier. Their study was developed experimentally using wind tunnels. Baldauf et al. [11] reported that the average concentration of NO_x and ultrafine particles near a large highway in Phoenix, Arizona, USA, was reduced from ~50% at 50 m downwind a noise barrier to about 30% at 300 m from the barrier. Recently, Venkatram et al. [12] studied the dispersion of pollutants in the crosswind direction of vertical barriers by means of a set of wind tunnel experiments. They found that downwind pollutant concentration tends to increase near the barrier crosswind edge but that the edge effects become negligible after a distance of seven times the barrier height.

Numerical studies: Other researchers have opted to study the pollutant dispersion phenomena by using numerical models based on computational fluid dynamics (CFD). Steffens et al. [13] reported a method to model green barriers in terms of the Leaf Area Density (LAD) which has been widely used to represent the effects of green barriers in CFD simulations. Using CFD, Steffens et al. [14] reproduced the 2008 NOAA experimental study finding that the presence of the barrier creates a much more complex flow downwind the road than without the barrier. They found that recirculation zones are formed in the wake of the barrier that is characterized by strong mixing regions.

The effect of changing the barrier configuration also has an impact on the distance from the barrier at which the concentration is significantly reduced [10]. These authors reported that the roadside barriers affect the dispersion of the vehicle-related-emissions in three ways: (i) they increase vertical dispersion through additional turbulence generated in the barrier wake, (ii) inducing vertical mixing behind the barrier in the cavity region, and (iii) they loft the emission above the barrier. Later, Adair and Jaeger [15] and Jin Jeong [16] used solid barriers and studied the effects on NO_x and CO concentration, finding reductions of the maximum wake concentrations of ~40 and ~70%, respectively. Morakinyo and Lam [17] furthered Steffens's studies by varying the distance between the vegetation barrier and the road. Then, Tong et al. [18] and Ranasinghe et al. [19] studied different alternatives combining both solid and green barriers and concluded that the most effective design to reduce pollutant concentration near roads is placing a solid barrier alongside a green barrier. Recently, Wang and Wang [20] studied the combined effect of the barrier and vehicle shape on the pollutant concentration over the road. They found that the flow recirculation zone was enhanced, increasing the road concentration levels. Soon after, Reiminger et al. [21] conducted a CFD study on the effect of vertical barriers on pollutant reduction under various atmospheric conditions, concluding that concentration reduction rates tend to increase from ~30 to ~60% as the atmospheric conditions become stable.

Huertas et al. [22] developed the near road CFD (NR-CFD) model, which simulates the dispersion of solid and gas-phase pollutants, over flat terrain, within a neutrally stratified atmospheric boundary layer, and includes the effect of turbulence and deposition on particle size distribution downstream. They found that pollutant concentration downwind the road exhibits a single profile when expressed in terms of three dimensionless numbers: normalized concentration, normalized distance to the road, and emission speed ratio. Recently, Huertas et al. [23] advanced this work and found that those pollutant concentrations vs.

distance to the road profiles are correlated to the ones obtained under different atmospheric stability conditions and reported the correction factor for each stability condition.

In the majority of the above-described studies, the barrier height was found to be the most significant influencer on the pollutant concentration, and therefore most of the studies focused on the effects of the barrier geometry only considered variations on the barrier height (Table 1). The exceptions to this trend were: (i) Busini et al. [24], who simulated the effect of using a barrier with a tilted section (45° from the vertical) on the dispersion of liquified natural gas (LNG) leaks from a straight pipe, finding said geometry to be the most effective at reducing the gas cloud size; (ii) Gerdroodbary et al. [25], who simulated the presence of a mesh barrier with holes of various sizes finding that the most effective results are obtained locating the barrier near to the road edge. It is important to note that in the aforementioned studies, barrier variations were evaluated independently.

Based on the reviewed references, the following areas of opportunity for improving the design of barriers for the mitigation of air pollution near roads were identified: (i) Consider the potential synergetic effects of the combined single-barrier variations among geometry, size, position, vegetative cover, and photocatalytic paints, among others; (ii) Quantify the effects of the barrier under different external conditions such as emission rate, wind speed, atmospheric stability conditions, among others; Include barrier cost in the design process; Report results in a generalized format in such a way that they can be used for applications beyond the specific modeled scenarios.

Aiming to address the needs stated above, the objective of this work is to quantify the effects of barrier geometry, size, and location on the dispersion of pollutants downwind an emission source, such as highway-type roads, located on flat regions in order to find the barrier that best reduces pollutant concentration at the lowest cost. In the process of pursuing this objective, the following main contributions to new knowledge were found: (i) By systematically using the calibrated NR-CFD model, the effects of the shape, size, and location of near-road barriers on the resulting ground pollutant concentration downwind a surface-emission source were quantified. Results were expressed in the way that they can be used for mitigating air pollution near any linear o area source of air pollutants; (ii) The ground pollutant concentrations downwind an emission source under any barrier geometry are highly correlated to the concentrations observed when there is not any barrier to the free wind flow. Furthermore, the parameters of the correlation for the case of simple barrier geometries of different sizes located at different distances from the road were reported; Different barrier designs were compared in terms of percentage of pollutant reduction and a metric related to the barrier cost. Results showed that the barrier with a quarter-ellipse geometry of a height equivalent to the 15% of the road width and located at the edge of the road is the best cost-effective design.

2. Methodology

Aiming to study the effects of the barrier geometry on the dispersion of the pollutants emitted from an area source located over a flat surface, (i) the dispersion of air pollutants emitted from a road located on a horizontal area without obstacles to the wind flow other than the barrier was considered as the case of study. Then, (ii) using CFD, the physics of the dispersion phenomena occurring in the near-ground atmosphere (<250 m high) were simulated in a small computational domain (<1 km long). (iii) The results from the simulation (NR-CFD model) were validated by comparing them with the experimental measurements. Then, (iv) the dispersion of pollutants emitted from the road was simulated considering different barrier geometries. Finally, (v) the simulated results were used to compare the concentrations downwind the road, under different barrier geometries with the ones observed under no barrier conditions and evaluated their cost. Next, each of these steps will be described.

2.1. Case of Study

In this work, the dispersion of the pollutants emitted from a road located on a flat region was studied, first without the presence of any obstacle to the wind free flow, and then considering the presence of different solid barrier structures located at different positions from the road in the downwind direction (Figure 1). This is an illustrative example of the general case, the dispersion of the pollutants emitted from an area source located over a flat surface.

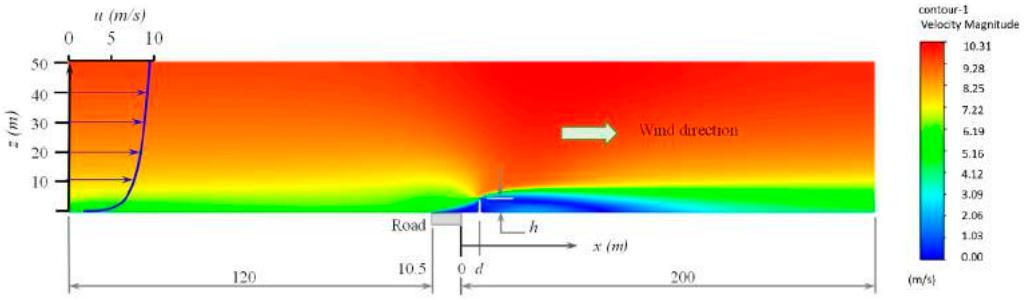

Figure 1. Computational domain considered in this study. Length scale is not uniform on the illustration.

The main area of interest is the region near the source and right after the barrier where people are exposed to the highest concentrations. This corresponds to the region near the ground surface (z < 250 m) and nearby the emission source (length < 1 km). Therefore, the problem domain shown in Figure 1 was considered, which is a box of 330.5 m and 50 m in the along-wind and vertical direction, respectively. These dimensions were selected according to Franke et al. [26], who recommended the minimum dimensions of the computational domain in the way that the walls do not interfere with the dispersion of the pollutants, even in the presence of obstacles. They recommended a minimum height of $6h$, where h is the characteristic length of the obstacle, which for this case, corresponds to the barrier height. According to the results obtained in a similar CFD study [23], the dispersion phenomena are symmetric in the crosswind direction, so a 2D computational domain was considered appropriate for this work. This 2D simplification implies that the barrier edge effects in the crosswind direction were not considered. This simplification is equivalent to considering infinitely long barriers in the crosswind direction or to studying a barrier segment that is far away from the barrier edge.

2.2. Barrier Configuration and Location

With the purpose of studying the effect of the barrier geometry on the dispersion of pollutants downwind the roads, three different geometric structures were considered: (i) a vertical straight barrier which is the most used shape in barrier studies, (ii) a 45° inclined straight barrier, which has shown a significative effect in pollutant dispersion [24], and (iii) a quarter-ellipse with zero eccentricity which is a shape found in some highway-type noise barriers. For the last two cases, the possibility that the barriers could be tilted towards and from the road was considered.

As mentioned before, height has been found to be the most significant variable affecting pollutant dispersion. As such, a set of barrier heights (h = 1.5, 3.0, 4.5, and 6.0 m) was considered. It is important to note that most transport agencies around the world recommend noise barriers to be at least 1.5m above ground in order to achieve satisfactory noise mitigation, however, additional factors such as visual impact, public privacy, shading, air circulation, and visibility must be also considered [27–29]. The 6.0 m case was of particular interest since the resulting pollutant concentrations can be directly comparable with the experimental measurements obtained in the Near Road Tracer Study (NRTS08) campaign [5]. The effects of the barrier location on pollutant dispersion were also studied. Barriers located at distances d = 0, 6, 10, 30 m downwind the road were considered.

2.3. Simulation of the Dispersion Phenomena (the NR-CFD Model)

The physics of the dispersion phenomena occurring in the near-ground atmosphere are described by the mass, momentum, and energy conservation equations [30]. Nevertheless, the task of solving these equations is challenging because they are nonlinear partial differential equations. For the purposes outlined above, the challenge is to reproduce the dispersion phenomena at the microscale level (<250 m high and <1 km long). This challenge has been tackled by solving these governing equations using the CFD technique. In CFD, the space domain (Figure 1) is divided into small volumes, and the governing equations are solved over each volume using a numerical technique called finite volume method (FVM). The simulation of the dispersion phenomena occurring in the atmosphere also requires the specification of the conditions under which the governing equations need to be solved.

The pseudo-steady-state assumption: In the study of pollutant dispersion, researchers are interested in short (~1 h) and long-term (~1 year) average results. As an approximation, the pseudo-steady-state approximation can be used. That is, the evolution of the atmosphere is considered as a succession of states where at each time interval, the atmosphere is assumed to be under steady-state conditions [23]. The previous assumption is valid if the time step of the simulation is smaller than the response time of the atmosphere to changes in radiative forcing, which is about 1 h, and it corresponds to the rate at which meteorological data is usually reported [31–33].

Following up the above argument, a steady-state condition was used. This pseudo steady-state assumption has the following implications for the modeling of the baseline case, i.e., pollutant dispersion over a flat surface without any perturbation to the wind free flow:

- The condition of horizontal homogeneity. The value of any property remains the same at any position with the same height.
- The inlet boundary condition should be known. At every vertical position at the inlet, the value of each variable should be a known input data.
- Agreement between the inlet and the ground boundary conditions. The condition of horizontal homogeneity requires that the ground boundary conditions for momentum and heat transfer agree with the inlet boundary conditions.

Next, the boundary conditions considered for the present NR-CFD model will be detailed. A particular emphasis will be given to the physics behind the used boundary conditions.

Inlet boundary conditions: The inlet boundary conditions for temperature, velocity, and turbulence are determined by the atmospheric stability condition. It describes the degree of thermal turbulence in the atmosphere, and therefore its capacity for transporting and dispersing pollutants [30]. Across the years, several scales and parameters have been defined and used by different field researchers to quantify and classify different stability conditions, with the Monin–Obukhov Length (L) [34] being one of the most popular. Huertas et al. [23] developed a pollutant dispersion study in which several L values were modeled using a similar computation domain as in this work. They found that, when using dimensionless numbers, ground pollutant concentration downwind an emission source under any atmospheric stability condition is highly correlated to the concentration observed under neutral conditions in a way that each stability case concentration can be computed from the neutral case by simply multiplying it by a corresponding stability factor *fs*, also reported in said work [23].

Therefore, for the present work, a neutral atmospheric stability condition was considered, corresponding to $L = -10^{100}$ m, which according to the 2-year observation by Zoras et al. [35] and the two-month period of experimentation from Finn et al. [5] is the most repeated condition.

In this work, the gained knowledge in the simulation of the atmospheric dynamics in a small computational domain was used. Specifically, the inlet boundary condition for speed and temperature profiles were established following up the Monin–Obukhov Similarity

(MOS) theory. This theory states that any mean flow quantity in the atmospheric surface layer (e.g., momentum or energy), when normalized by an appropriate scaling parameter, is a unique function of $\zeta = z/L$ where ζ is known as the buoyancy parameter [30], and L is the Monin–Obukhov length, which describes the atmospheric stability condition. Based on the observation that (i) in the atmospheric surface layer (ASL) the wind speed (u) varies logarithmically with height 0, and that (ii) the surface roughness forces the mean wind speed to be zero at the ground surface, the MOS theory states that the vertical profiles of both wind speed and temperature in the ASL follow a logarithmic form that depends on L [32]. The resulting vertical profiles of wind speed and temperature for $L = -10^{100}$ m were used as the inlet boundary conditions. It is important to note that for a neutral condition, the temperature profile is invariant with height.

Other boundary conditions: A wall boundary condition was used for both, the ground and barrier boundaries. Following the $y+$ metric, the simulation of wind flow over a flat surface required finite volumes of ~1 cm near the ground surface. As described before, the height of the computational domain was selected as the minimum where vertical interaction (other than turbulences) is negligible. Then, following best CFD practices, the symmetry condition (zero gradients) was selected as the upper boundary condition. A uniform velocity inlet at the road was specified to physically represent that the incoming wind flow faces a perpendicular wind flow with a high pollutant concentration (the source of pollutants). For the outlet condition, a pressure outlet condition of 1 atm was defined, which is valid considering the small height of the domain and the invariant temperature profile used. An adiabatic condition was used for the ground boundary.

Turbulence model: Turbulence models for the ASL should account for both shear and buoyancy produced turbulence [36]. Best results in the use of CFD have been obtained in capturing the turbulence phenomena by solving these equations with a high time and space resolution. This approach, known as direct numerical simulation (DNS), is computationally expensive and therefore has not been used to systematically study pollutant dispersion [37]. As an alternative, models that describe average-flow quantities, such as the Reynolds-Average Navier Stokes (RANS) approach, have been considered instead. In particular, the k-ε turbulence model has been widely used for modeling the ASL [38]. The k-ε model adds an equation for the turbulent kinetic energy (k) and an equation for the turbulent energy dissipation (ε). Both equations ensure the closure of the system of governing equations describing the atmospheric dynamics on the ASL. Most of the work dedicated to simulating microscale pollutant dispersion uses this model while also assuming isotropic turbulence, which are features of a neutral atmosphere [14,22,39]. Pieterse and Harms [36] measured k and ε at different heights for several atmospheric stability conditions on flat terrain without obstacles to the wind flow. They proceeded to simulate the wind flow via CFD, reproducing those experimental results by fixing average values for k and ε at the inlet boundary conditions (k = 1.2699 m^2/s^2 and ε = 0.000544 m^2/s^3 for the neutral stability) and specifying values for the coefficients found in the k-ε formulation that were dependent on both height z and Monin–Obukhov length L [38]. This methodology was adopted for the present work to describe the turbulence within the chosen atmospheric stability condition, and the k and ε average values reported by them were also used for the inlet boundary condition.

Simulation of the pollutant dispersion: Vehicle transit over roads generates pollutants that are emitted both directly from the vehicle's tailpipe and from the road-wheels interaction. Attempting to deal with the complexity of the real air pollutant dispersion, researchers have subdivided its study in three phases [39]: From the source (tailpipe or wheel-road interaction) to the ambient near the vehicle, where solid and gas phase pollutants maintain their characteristics with a dilution ratio of up to 1000:1. Then, from the vehicle to the road, where pollutants mix with other sources of pollutants with a dilution ratio of up to 10:1, and then from the road to the ambient downwind the road.

Focusing this work on the last phase, a uniform concentration on the road was assumed as a net result of the multiple vehicles crossing by the same position over a long

time, regardless of the exact source of the pollutants. For comparative purposes, an arbitrary emission of $E = 1$ g s^{-1} m^{-2} was chosen, verifying that results do not depend on the emission rate [22]. Chemical reactions were not considered in this model, which is acceptable for the case of inert pollutants or pollutants with a mean lifetime significantly longer than the residence time within the computational domain. In our case, for a wind speed of 1 m/s, the residence time of gas-phase pollutants in the computational domain is ~5.5 min.

In order to model gas-phase pollutants dispersion, a species transport model was added to our CFD simulation. It solves the conservation equations for each of the chemical species in the computational domain and predicts their local mass fraction across said domain [40]. Thus, the model integrates a convection–diffusion equation (Equation (1)), as well as a mass diffusion flux equation for turbulent flows (Equation (2)) during the iterative solution process.

$$\frac{d(\rho Y_i)}{dt} + \nabla\,(\rho u Y_i) \;=\; -\nabla\, J_i + R_i + S_i \tag{1}$$

$$J_i \;=\; -\left(\rho D_{i,m} + \frac{\mu_t}{Sc_t}\right)\nabla Y_i - D_{T,i}\frac{\nabla T}{T} \tag{2}$$

In Equations (1) and (2), u is the fluid velocity field, Y_i is the local mass fraction for species i, J_i is the diffusion flux of species i, R_i is the net production rate of species i by chemical reaction, S_i is the generation rate from the dispersed phase plus user-defined sources, ρ is the bulk fluid density, μ_t is the turbulent viscosity, $D_{i,m}$ is mass diffusion coefficient for species i in the mixture (defined as 9×10^{-6} m^2 s^{-1} for free SF_6-air diffusion [41], $D_{T,i}$ is the thermal (Soret) diffusion coefficient for specie i, which can be neglected for the present case, and T is the bulk fluid temperature [40]. Bold symbols are vectors. For the present model, the species considered were dry air and SF_6. This last one is a tracer gas known for its high density compared to air and its easily detectable nature even at low concentrations. This gas-phase pollutant surrogate was chosen to directly compare the NR-CFD model to the experimental results of the NRTS08 campaign.

Other details of the CFD model: The solver used for the present study was the commercial software ANSYS FLUENT v2020. A pressure-based solver was used with a coupled scheme, in which, the mass and momentum equations are solved simultaneously while the other equations (energy, species transport and turbulence) are solved segregated. Even though the effects of the gravity were included in the simulation, no evidence of a strong influence of this term was observed in the solution. Second order schemes were used in the spatial discretization of all the equations. The convergence criteria for all the equation were set to 1×10^{-6} and a maximum of 5000 iterations were run for the finest mesh. A hybrid initialization scheme was used for all the cases that were run; this type of initialization is prefer since it allows a faster convergence of the numerical results.

Convergence and grid independence analysis: For the case of no-barrier presence, quad-type elements were used to discretize the general domain. Grid refinement was performed near the domain walls. The height of the first cell was 0.01 m, which is equivalent to a $y+$ value of 150. This value satisfies the log-law of modeling that recommends $30 < y+ < 1000$ [42]. The overset meshing method was used aiming to mesh the different barrier geometries considered. This technique consists of partitioning and meshing certain regions of a given domain separately and then overlapping them so that their solution data can be interpolated [43]. This technique reduces the computational costs of meshing a domain each time a specific zone or a geometrical detail of said domain is changed. Thus, the general domain shown in Figure 1 was divided, partitioning the area near to the barrier and establishing its limits as an overset boundary condition while leaving the rest of the region as the "background mesh" with the previously described parameters. This allowed to individually mesh only the near-barrier region of the domain, which was considered of size $6\,h \times 7\,h$ [26], where mesh cells that could change as an effect of changing the geometry of the barrier and or moving it across the domain are affected (Figure 2). The boundary conditions of the overset partition were established as Overset in the CFD solver, ensuring

the interpolation of information from the cells in the overlapping areas. The height of the first cell was 0.001 m for the overset barriers, which is equivalent to a $y+$ value of 30 [42]. Figure 2a shows the complete mesh in which the size of the elements cannot be seen due to the size of the scale. The background mesh is in green while the near-barrier mesh is in blue and the overset boundary is the black solid line. Figure 2b shows a view close to the barrier in which the size of the elements is now observable, especially of the background mesh. The overlap of the two meshes is also shown. Finally, Figure 2c shows a close up view of the mesh at the tip of the barrier in which is clear the refinement close to the barrier in order to correctly resolve the turbulent boundary layer. It can be also observed that the cells mainly grow in the direction normal to the wall.

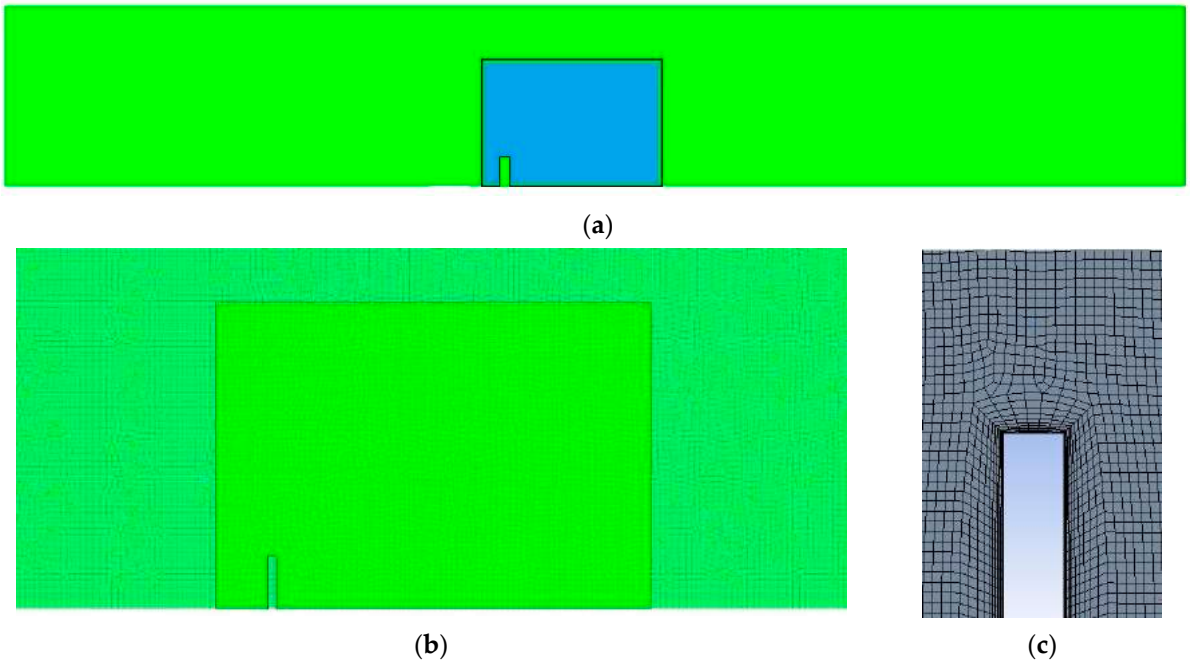

Figure 2. Illustration of the overset technique for the discretization of the computational domain (**a**) complete mesh, (**b**) detail of the mesh close to the barrier and (**c**) detail of the mesh close to the tip of the barrier.

A mesh of 0.421 million of elements was used for the simulations, including the overset and the refinements. The background mesh has 0.343 million of elements while the near-barrier mesh has approximately 0.078 million of elements. This mesh was selected after a grid independence analysis from using five different meshes with total number of elements ranging from 0.02 to 1.0 million elements, using as criteria pollutant downwind concentration and vertical wind speed profile. On a server with 16 parallel processors, solution times ranged from 30 min to 4 h for the finest mesh.

2.4. Use of Dimensionless Numbers to Study the Effect of Barrier Geometry on Pollutants Dispersion

Following the work of Huertas and Prato [22], the effects of emission rate, wind speed, and road width were isolated on the model results by reporting them in terms of a set of dimensionless numbers. Huertas and Prato [22] demonstrated that, for neutral atmospheres, when pollutant concentrations downwind the road are expressed in terms of the dimensionless numbers for concentration (C^*, Equation (3)) and distance to the road (x^*, Equation (4)), the resulting profiles are independent of wind speed (U), emission rates (E), road width (w) and the nature of the pollutant. The Schmidt number (S_c) in Equation (3) takes into consideration the diffusive properties of the pollutant on its dispersion. Therefore, variations found on that universal profile will be attributed to variations on the barrier geometry rather than just variations on these variables. For this particular

work, a dimensionless barrier height (h^*, Equation (5)) and distance (d^*, Equation (6)) were also defined in order to account for the different barrier heights and distances from the road considered.

$$C^* = \frac{C\,U}{E} S_c \tag{3}$$

$$x^* = \frac{x}{w} \tag{4}$$

$$h^* = \frac{h}{w} \tag{5}$$

$$d^* = \frac{d}{w} \tag{6}$$

where w is the road width (10.5 m), S_c is the Schmidt number, which is used to characterize pollutant diffusive properties. It is important to note that the wind speed (U) used for Equation (3) corresponds to the wind speed measured in the profile at 10 m height, which is the standard reference height above ground level for wind measurements in open fields according to the World Meteorological Organization (WMO) [44].

2.5. Validation with Experimental Results

In order to validate the CFD-based model for the dispersion of pollutants near roads (NR-CFD model), the results obtained from this model were compared with the experimental data obtained in the Near Road Tracer Study (NRTS08), with and without a 6 m tall barrier. Said study was conducted in 2008 by the NOAA, Idaho National Laboratory (INL), Air Resources Laboratory (ARL), and Environmental Protection Agency (EPA) in Idaho Falls, USA [7] and reported by Finn et al. [5] and Steffens et al. [14]. Figure 3 illustrates the experimental setup implemented. They released a 1 g s^{-1} constant flow of a tracer gas (SF_6) distributed uniformly along a 54 m line and used an array of bag samplers to measure the 15 min average SF_6 downwind concentrations at 3, 4, 6, 8, 11,15, 20, and 30 times the road width. They adopted an equivalent road width of 6 m in their experiments. Anemometers were placed at several vertical positions to measure wind speed, wind direction, turbulence characteristics, friction velocity, heat flux, and atmospheric stability. The tests were repeated under different atmospheric conditions when the wind flowed nearly perpendicular to the line emission source. Each test lasted around 3 h, resulting in a total of 10–12 measurements for each position considered.

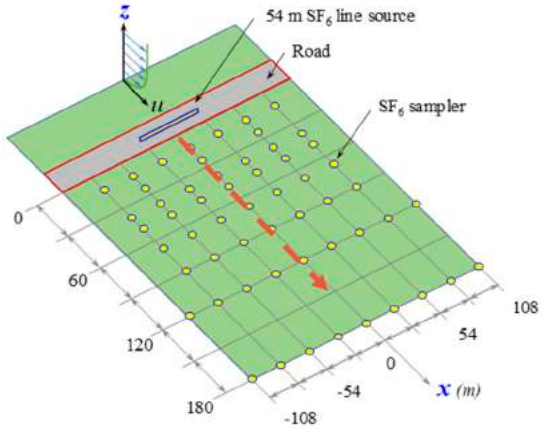

Figure 3. Illustration of the experimental setup implemented during the Near Road Tracer Study (NTRS08) campaign in Idaho Falls, USA. In this study, results obtained with and without a 6 m straight barrier were used.

Even though their interest was the study of the effects of a side road 6 m high straight barrier on the dispersion of pollutants, they also carried out several tests without any barrier to the wind free flow under different atmospheric stability conditions. Time and test average values of both sets of data that were taken in neutral atmospheric conditions

and over the centerline of the crosswind direction downwind the road (see dotted line in front of the line source in Figure 3) were used for a comparative analysis, as it was the line with the highest measured concentration values. A Schmidt number for SF_6 of 0.207 was considered to express their experimental results in terms of C^* (Equation (3)).

2.6. Barrier Cost Evaluation

In order to include the barrier costs in the barrier design process, a simple qualitative cost model (S_r, Equation (7)) was defined based on the barrier height (h) and a cost factor (C_b). Equation (7) assumes that cost increases linearly with barrier height, regardless of the geometry complexity. S_r is dimensionless variable that compares the cost of the barrier under consideration with respect to the cost of a 1 m high straight barrier. This model evaluates the barrier cost without directly considering the material, manufacturing, and installation cost, which can significantly vary between regions. In Equation (7), C_b, with units of m^{-1} (score per meter), assumes that the barrier cost increases with the complexity of the barrier geometry. C_b values were defined for the different modeled barrier geometries according to their complexity, where a simple straight barrier was considered as the base case (C_b = 1), a straight inclined barrier had a larger C_b than a straight barrier (C_b = 1.2), but smaller than the quarter-ellipse barrier, which has a higher expected manufacturing cost than the rest ($C_b = 1.5$).

$$S_r = C_b\, h* \tag{7}$$

It is important to note that, while this model does not account for the nonlinear cost structure that would be expected in real manufacturing, it does offer a basic framework to hierarchically compare the different barrier configurations modeled in a cost-benefit analysis.

3. Results and Discussion

3.1. Comparison with Experimental Results

Aiming to validate the capacity of the NR-CFD model of reproducing experimental measurements, the NR-CFD model was used to simulate the dispersion of SF_6 under the same conditions that the experimental tests were conducted with and without a 6 m vertical barrier, using as input only the data points of speed and temperature measured by the meteorological station at 10 m height. Then, the experimental results of C^* were compared with the results of C^* obtained by the NR-CFD model for identical positions downwind the road and under neutral atmospheric conditions (Figure 4a). A high correlation ($R^2 > 0.96$) was observed between the C^* simulated and C^* experimental (and with slopes close to one (Figure 4b) for both cases, with and without barrier. These results demonstrate the capacity of the NR-CFD model of reproducing short-term experimental measurements.

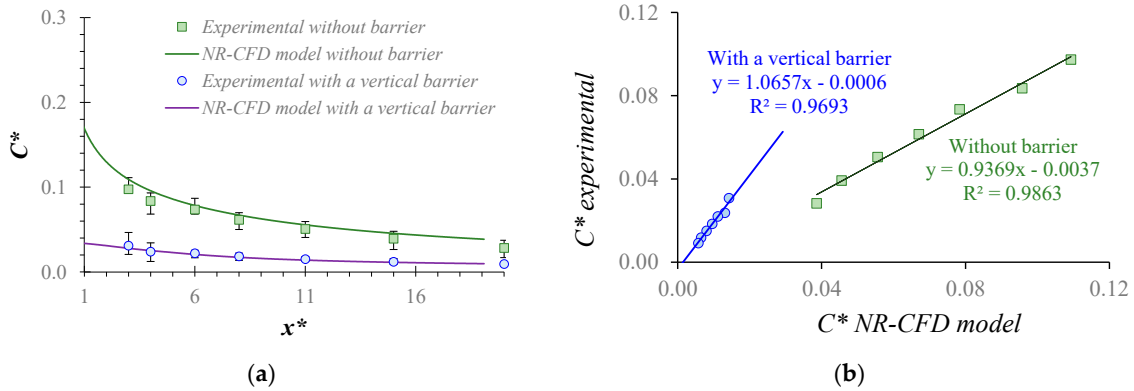

Figure 4. Comparison of the results obtained by the near road CFD (NR-CFD) model with the experimental measurements obtained in the NRTS08 campaign. (**a**) SF_6 concentrations at several distances downwind a line emission source, under neutral atmospheric stability conditions, with and without a 6 m straight barrier. Circle and square markets indicate the average values, while vertical lines indicate the range of variation of the 18 experimental measurements. (**b**) Correlation analysis between the simulated and experimental results.

3.2. Resulting Velocity Contours

Aiming to observe the effect of the different barrier geometries on pollutant dispersion, the calibrated NR-CFD model was systematically used to simulate the dispersion of SF_6 and NO_x under the presence of the six barrier geometries considered. Initially, all barriers have 6 m and were located at 6 m from the road edge.

Figure 5a–g show the wind speed variations across the modeled domain near the barrier region obtained for the case of no barrier and for the six instances of barrier geometries considered. Figure 5a shows the small perturbation to the wind flow caused by the pollutants emitted at the road surface. This profile is significantly altered by the presence of the barriers. Overall, two distinctive regions can be distinguished: upwind and downwind the barrier. In each region, a low-speed recirculation zone is formed next to the barrier, whose sizes and shapes depending on the barrier geometry. Large and tall downwind wakes are desired because they contribute to the pollutant dispersion and, therefore, to the reduction in near-road ground pollutant concentration. In this sense, the quarter ellipse oriented toward the road offers the best performance. However, upwind the barrier, low-speed recirculation areas are desired as they contribute to pollutant accumulation on the road. Barriers oriented downward the road offer the best dilution effects on the road.

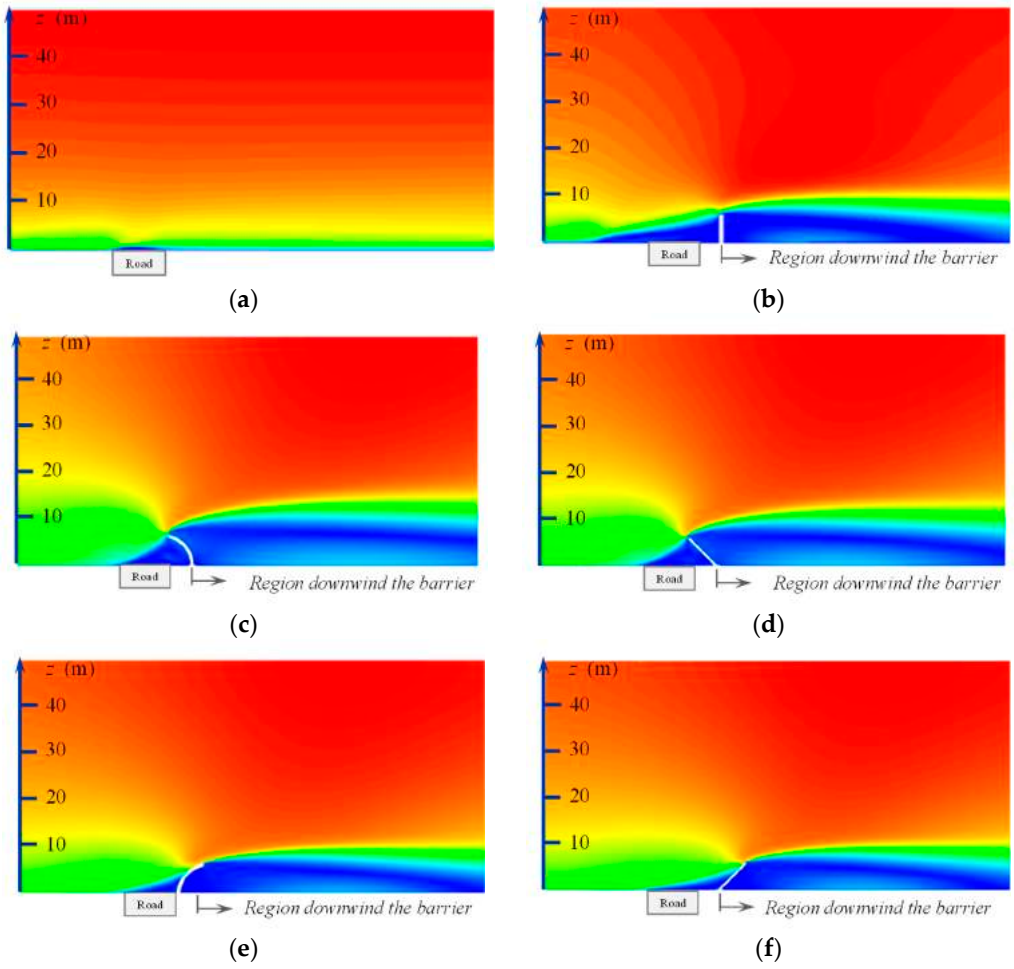

Figure 5. *Cont.*

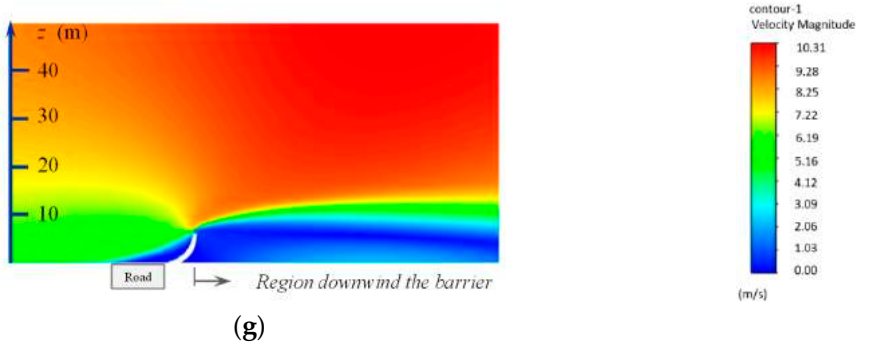

(**g**)

Figure 5. Contours of wind speed obtained by the NR-CFD model simulating the dispersion of pollutants emitted from a road located on flat terrain, under neutral atmospheric conditions, $E = 1\ g\ s^{-1}\ m^{-2}$ and $U = 7.65$ m/s. (**a**) Without any barrier. Under the presence of (**b**) a vertical straight barrier, (**c**) a quarter-ellipse barrier oriented toward the road, (**d**) a straight barrier inclined 45° toward the road, (**e**) a quarter-ellipse barrier oriented downward the road, (**f**), a straight barrier inclined 45° downward the road, and (**g**) an inverted quarter-ellipse barrier oriented downward the road. All barriers are $h^* = 0.57$ in size and are located at $d^* = 0.57$ from the road.

3.3. Vertical Mass Flux Profiles

Then, the horizontal mass flux as a function of height was computed at several distances downwind the barrier (Figure 6). Said fluxes indicate the amount of pollutant per unit area that flows across a vertical plane as a function of height. Under steady conditions, the total mass flux of pollutants should remain the same at every location downwind the barrier when deposition or any mechanism of pollutant depletion is not considered. Under these considerations, the area between the vertical axis and the curve should be one when the mass flux is normalized by the total mass flux.

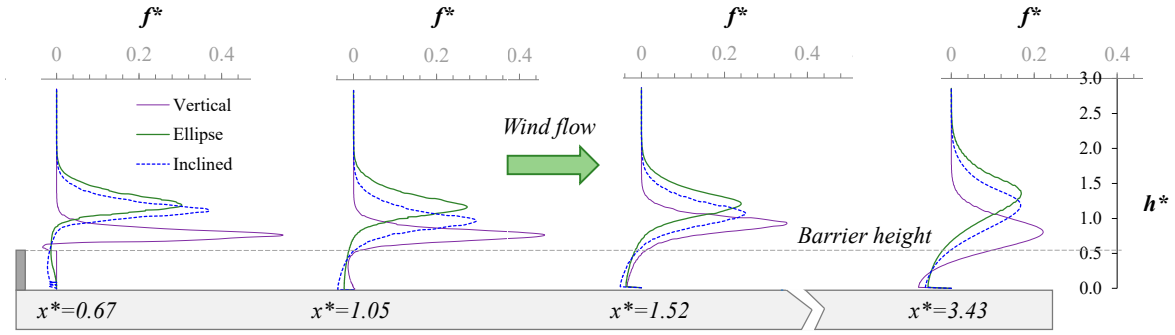

Figure 6. Vertical profiles, at several distances downwind the barriers, of SF_6 mass fluxes developed by 6 m elliptical, vertical and inclined barriers located at 6 m downwind the road ($d^* = 0.57$), for the case of neutral atmospheric conditions, $E = 1\ g\ s^{-1}\ m^{-2}$ and $U = 7.65\ m\ s^{-1}$.

A negative flux indicates pollutant recirculation. It is an undesired effect for the sake of dispersing pollutants as it could lead to pollutant accumulation. To enhance dispersion, barriers should develop vertical flux profiles with the widest peak at the greatest height possible. The height of the peak indicates the barrier ability of lofting the pollutants, and the wide of the peak indicates its ability to disperse pollutants in the vertical direction. Figure 6 shows that the quarter ellipse oriented toward the road exhibit the best performance in dispersing pollutants.

3.4. Effect of the Barrier Geometry and Size on Ground Pollutant Concentration

Next, the calibrated NR-CFD model was used to quantify the effects of the barrier size and geometry on the pollutant concentration upwind and downwind the barrier. As

previously found by [22], studying the dispersion of pollutants near roads for the case without barriers, when the downwind concentrations are expressed as C^* vs. x^*, the resulting profile is unique. It is independent of the parameters such as wind speed, pollutant emission rate, and even the nature of the pollutant substance. Hence, the barrier dispersion performance will be reported in terms of these dimensionless variables (Equations (3)–(6)).

As stated before, the analysis begun by fixing the barrier location at a 6 m downwind the road ($d^* = 0.57$). Figure 7a–f show the ground pollutant concentration as a function of distance to the road (C^* vs. x^*) obtained for the different barrier geometries considered and for different barrier size. It is important to highlight that even though the results shown in Figure 7a–f were obtained for SF_6, these results are valid for any gas-phase pollutant, under any condition of emission rate and wind speed, when the atmosphere is neutrally stratified.

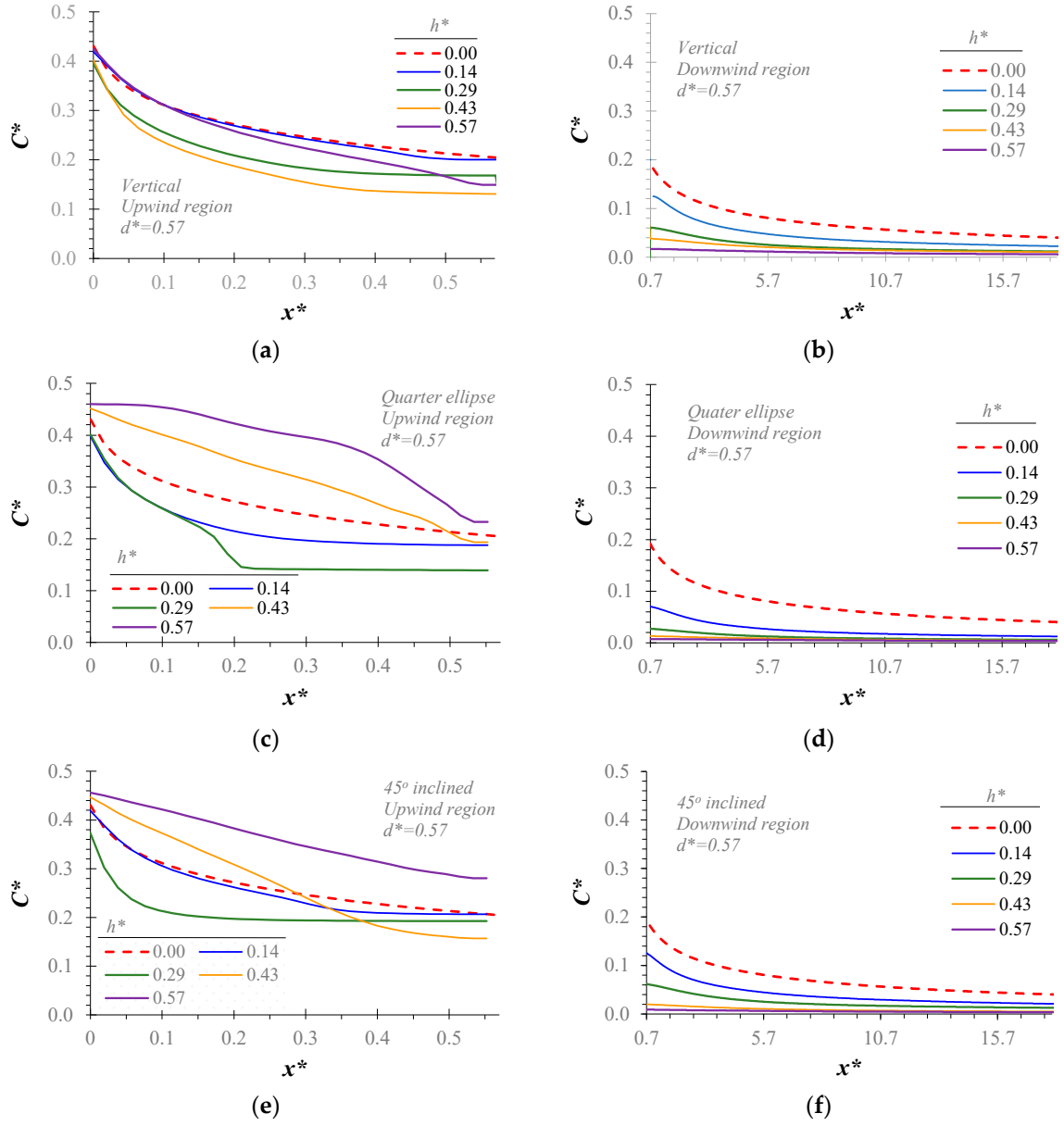

Figure 7. Pollutants ground concentration as a function of barrier geometry and size, for the case of a straight vertical barrier (**a**) in the upwind region ($0 < x^* < 0.57$) and (**b**) in the downwind region ($x^* > 0.68$), a quarter-ellipse barrier oriented toward the road (**c**) in the upwind region and (**d**) in the downwind region, a 45° inclined straight barrier oriented toward the road (**e**) in the upwind region and (**f**) in the downwind region. Barriers are located at $d^* = 0.57$and its thickness covers the range $0.57 < x^* < 0.67$.

Figure 7a shows that, for the case of the vertical barrier, the pollutant concentration in the upwind region ($x^* < 0.57$) remains below the reference case independently of the barrier height. For the geometries oriented towards the road (Figure 7c,e), the presence of the barrier increases the pollutant concentrations in the upwind region with respect to the case of no barrier. This effect is attributed to the tendency of pollutants to accumulate in the upwind region for those specific barrier shapes. However, a well-defined pattern could not be identified in the increase in pollutant concentration with the barrier size. It is important to remember that the main purpose of the barrier is to protect the people living in the region downwind the barrier ($x^* > 0.68$). Therefore, it is the region of primary interest in the design of road barriers.

Figure 7b,d,f show that in this region, the presence of the barriers reduces the pollutant concentrations compared to the case of no-barrier (dotted lines) and that this reduction increases with the barrier size. This qualitative result agrees with previous experimental and analytical results reported in several authors (Table 1).

Aiming to quantify the reduction effects, we notice that the concentration profiles, near to the road seem to be correlated to the concentrations obtained without any barrier (Figure 7a,b,f). Aiming to confirm these hypotheses, results for the downwind concentrations obtained for the case of no-barrier were selected as the base case of comparison, and correlation analyses with the results obtained under the other scenarios were carried out. Results confirmed this hypothesis. Figure 8a shows that near the barrier, in the downwind region ($0.68 < x^* < 5$, region with the largest concentrations), pollutant concentration obtained with different barrier geometries are highly correlated ($R^2 > 0.86$) with the one obtained without any barrier.

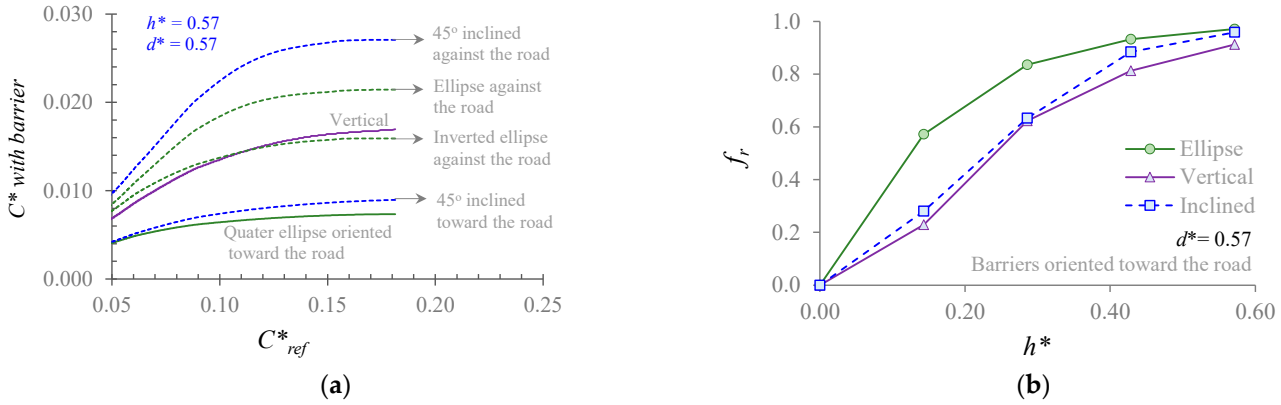

Figure 8. Quantification of the effects of the barrier geometry and size on the ground-level pollutant concentration observed in the region downwind the barrier ($x^* > 0.68$). (**a**) comparison of the concentrations observed with the barrier geometries with respect to the reference concentrations (case without any barrier). (**b**) Concentration reductions as a function of the barrier normalized size (h^*) for some of the barrier geometries considered. Barriers were located at $d^* = 0.57$.

For the case of the vertical barrier, a slope of ~0.087 was obtained in the correlation analysis, which means that the presence of the 6 m straight vertical barrier leads to downwind concentrations ~91% lower than the observed without any barrier. It also means that the presence of the barrier does not generate peaks of pollutant concentration downwind the barrier. The concentration always tends to reduce, following the same trend that for the case without the barrier.

The slopes of each correlation analysis were named as the ground concentration ratio (C^*/C^*_{ref}) and f_r (Equation (8)) as the barrier-induced concentration reduction factors.

$$f_r = 1 - \frac{C^*}{C^*_{ref}} \quad (8)$$

Figure 8b shows that when a 6 m quarter-ellipse and a 6 m inclined barrier oriented toward the road were used, the pollutant concentrations exhibited f_r~97% and f_r~96%, respectively. Reductions obtained with the same barriers, but oriented against the road, were f_r~88%, f_r~92%, and f_r~84%, for the quarter ellipse, inverted quarter ellipse, and inclined barrier, respectively. Previous results demonstrate that for 6 m barrier sizes, located at 6 m from the road (d^* = 0.57) the quarter ellipse oriented toward the road exhibits the best performance dispersing pollutants near the road. Then, the effect of the barrier size was studied. Figure 8b confirmed that, for any barrier geometry, f_r increases with barrier size. However, reductions in pollutant concentration (f_r) do not vary linearly with the barrier size. This figure also confirmed that the quarter ellipse barrier exhibits the best performance dispersing pollutants for all barrier sizes. Nonetheless, this superior performance becomes negligible among barrier geometries for sizes greater than 0.6 ($h^* > 0.6$).

3.5. Effect of the Barrier Location on Ground Pollutant Concentration

Then, the effects of varying the barrier location on its ability to disperse air pollutants were studied. Figure 9a shows f_r as a function of barrier location (d^*) and size (h^*) for the quarter ellipse barrier oriented toward the road. Figure 9b reproduces Figure 9a in its two-dimensional form. These figures show that f_r increases with h^* but decreases monotonically with d^*. Again, the base case is when there is not any barrier ($h^* = 0$) and therefore $f_r = 1$. Similar results (Figure 9c,d) were obtained for the case of the inclined and vertical straight barriers.

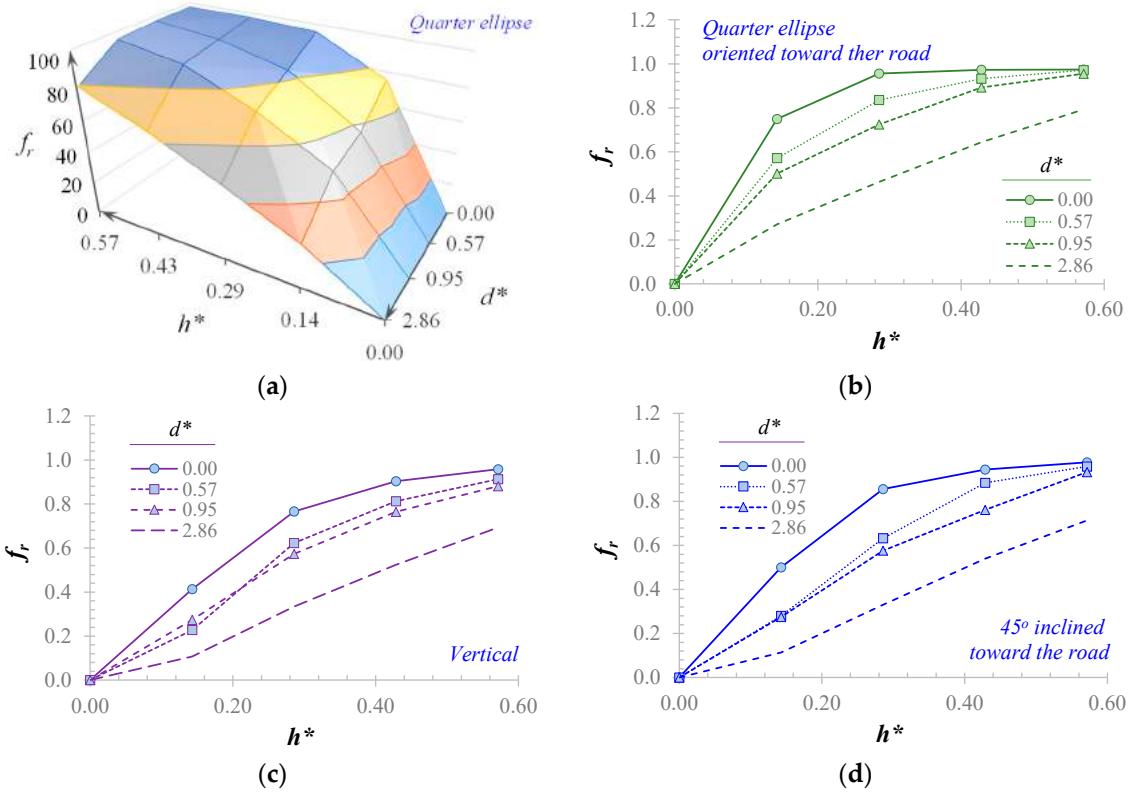

Figure 9. Concentration reduction factor (f_r) in the region downwind the barrier, as a function of barrier height (h^*) and location (d^*) for a quarter ellipse barrier in (**a**) a 3D plot and (**b**) a 2D plot; and 2D plots (**c**) for the vertical and (**d**) 45° inclined barrier. Barriers are oriented toward the road.

Then, it can be concluded that, regardless of the barrier geometry, the greatest reduction occurs when the barrier is located at the edge of the road ($d^* = 0$). In the situations that the barrier should be located down downwind the road, for example, to include a safety

sideline for the vehicles, the quarter ellipse inclined toward the road continues being the best barrier geometry, independently of how far downwind the road it should be located.

Previous results are difficult to compare with the reported by other authors (Table 1) since the reductions in pollutant concentrations obtained with the barriers depend on barrier geometry (height, distance to the road, and shape), meteorological conditions (wind speed, atmospheric stability), and emission rates, and in most of the cases these variables have not been reported. These dependence on multiple variables explain the differences in the results reported in the works listed in Table 1.

3.6. Including Cost in the Selection of Barrier Size and Geometry

Figure 10 shows the dispersing performance of the barrier geometries considered in this study when they are located at the road edge ($d^* = 0$) as a function of the barrier size (h^*). We highlight that in this figure, the air pollutant dispersing performance of the barrier is expressed as the fraction of the downwind ground concentrations (C^*/C^*_{ref}). Therefore, the best performance is observed when this ratio tends to zero.

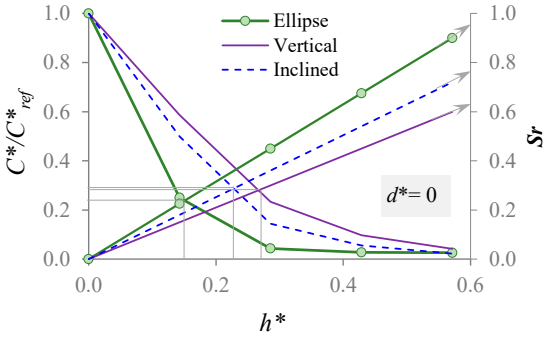

Figure 10. Dispersing performance measured as (C^*/C^*_{ref}) and relative cost (S_r) of different barriers located at the road edge ($d^* = 0$) as a function of the barrier size (h^*). Intersections indicate the barrier size with the most favorable cost-benefit ratio for each barrier geometry considered.

Figure 10 also includes the relative cost (S_r) calculated as described in Section 2.6. This figure also shows that the rate of gain in the dispersing performance with respect to the barrier height ($d(C^*/C^*_{ref})/dh^*$) tends to decrease with h^*. However, the rate of cost increment (dS_r/dh^*) remains constant. Therefore, for a given barrier geometry, the intersection of the C^*/C^*_{ref} curve with its corresponding S_r line qualitatively represents the barrier size with the most favorable cost–benefit ratio. Larger barriers require greater economic resources per unit of dispersing performance gained.

According to the above reasoning, the best cost-effective dispersing barrier has a geometry of a quarter ellipse oriented toward the road with a height of h^*~0.155 (h~1.62 m for a road 10.5 m wide) and located at the road edge. This barrier reduces 76% of the concentration observed near the road without any barrier. It is important to note that this alternative achieves higher pollutant reduction percentages than what has been typically reported for vertical barriers in the presence of gas phase pollutants [11,15,21].

Similar dispersing capacities can be obtained with the vertical barrier. However, it requires a larger barrier ($h^* = 0.29$ or h~3.05 m for a road 10.5 m wide) with a slightly higher relative cost ($S_r = 2.8$) than for the case of the quarter ellipse barrier ($S_r = 2.4$).

The above analyses are general recommendations in the design of barriers for mitigating the pollution near roads. However, the final design of the barriers needs to include additional considerations such as local aspects (actual barrier construction cost) and other specific needs (minimum and maximum distances to the road, feasibility for vehicles to get close to the barrier, etc.).

Results reported in this work can be used in multiple applications such as traffic-related emissions, industrial gas pipe leaks, and in general, any area or line-source of pollutants emitted on flat terrain. Results may be used to quantify the exposure level to

air pollutants of the population living near highway-type roads, as well as to identify effective countermeasures to mitigate the impact of said pollutants. It is important to note that the study of synergic effects of additional barrier properties such as vegetative covers, structural holes, and the use of pollutant-absorbent or catalytic paints are outside the scope of this work. Additional work is required to confirm that results obtained in this study, when expressed in dimensionless numbers, are independent of the road width. Barrier edge effects in the crosswind direction were neither considered in this study.

4. Conclusions

Solving numerically, via CFD, the governing equations that describe the dispersion of air pollutant emitted by the transit of vehicles in roads in the near-ground atmosphere under neutral conditions, the effects of the presence of solid barriers on the nearby resulting concentration were systematically evaluated. The use of dimensionless numbers ensured that variations observed on the obtained downwind concentration profiles (C^*) were attributed solely to variations on the barrier size, geometry, or location considered.

It was found that the resulting near road CFD model (NR-CFD model) produce results that agree ($R^2 > 0.96$) with the experimental results obtained by the NOAA in 2008 observing the SF_6 concentrations at several distances downwind a line source of SF_6, for the cases of a 6m straight barrier and for the case of no barrier.

It was observed that the experimental and modeled C^* obtained under different barrier geometry conditions are highly correlated ($R^2 > 0.86$) to the C^*_{ref} (C^* observed under no barrier conditions). The slope obtained from the correlation analysis was named as concentration ratio (C^*/C^*_{ref}) and $f_r = 1 - (C^*/C^*_{ref})$ as the barrier-induced concentration reduction factors.

It was observed that, regardless of the barrier geometry, the downwind concentration reduction (f_r) increases with the barrier size and decreases with distance to the road (d^*). They met their maximum performance when they are located at the road edge ($d^* = 0$). Under all circumstances, the quarter ellipse oriented toward the road exhibited the best performance. However, the outstanding performance of this barrier configuration becomes negligible compared to other geometries when the barrier size is larger than $h^* > 0.57$ (6 m for a 10.5 m road width), and the barrier are very near to the road edge. Under these circumstances ($d^* = 0$ and $h^* > 0.57$), all barrier configurations reach an fr~98%.

It was assumed that the manufacturing and installation costs of the barriers increase proportionally to their size and to the complexity of its geometry. Therefore, a barrier with a quarter ellipse geometry and a 45° inclined straight barrier cost 1.5 and 1.2 times the cost of a vertical straight barrier, respectively. Then, it was found that the barrier with the best-dispersing capacity per unit cost has a geometry of a quarter ellipse oriented toward the road with a height of h^*~0.155 (h~1.62 m for a road 10.5 m wide) and located at the road edge. This barrier reduces 76% of the concentration observed near the road without any barrier.

The results obtained in this study may aid in the decision-making process of industrial, research, or government institutions for the selection and design of solid barriers as pollutant mitigating infrastructure near any area-source of pollutants, located over a flat area, such as leakages from pipes, particle resuspension due to wind erosion, open burning, etc. It is important to note that even though results are valid for any non-chemically reactive gas-phase pollutant, they are valid only for the case of emission sources located on flat terrain with the barrier as the only obstacle of the wind free flow. Barrier edge effects in the crosswind direction are not considered in this study. Additional work is required to confirm that results obtained in this study, when expressed in terms of dimensionless parameters, are independent of the road width since said parameter was not systematically varied in this work.

Author Contributions: Conceptualization, J.I.H.; methodology, J.I.H. and O.D.L.M.; simulation, J.E.A. and Cristian H. Lopez; validation, J.E.A.; formal analysis, J.I.H., J.E.A. and Cristian H. Lopez; literature review, J.E.A. and C.H.L.; data curation, J.I.H.; writing—original draft preparation, J.I.H. and J.E.A.; writing—review and editing, J.I.H., J.E.A. and O.D.L.M.; supervision, J.I.H. and O.D.L.M. All authors have read and agreed to the published version of the manuscript.

Funding: This research received no external funding.

Institutional Review Board Statement: Not applicable.

Informed Consent Statement: Not applicable.

Data Availability Statement: The data presented in this study are available on request from the corresponding author. The data are not publicly available due to privacy reasons.

Acknowledgments: This study was partially financed by the Mexican Council for Science and Technology (*CONACYT*) and Tecnológico de Monterrey. The authors also acknowledge the contributions to this work of MSc. Sebastian Martinez from Tecnológico de Monterrey.

Conflicts of Interest: The authors declare no conflict of interest.

References

1. Karner, A.A.; Eisinger, D.S.; Niemeier, D.A. Near-Roadway Air Quality: Synthesizing the Findings from Real-World Data. *Environ. Sci. Technol.* **2010**, *44*, 5334–5344. [CrossRef] [PubMed]
2. Singh, S.; Adams, P.J.; Presto, A.A. Simulations of vehicle-induced mixing and near-road aerosol microphysics using computational fluid dynamics. *AIMS Environ. Sci.* **2018**, *5*, 315–339. [CrossRef]
3. Nitta, H.; Sato, T.; Nakai, S.; Maeda, K.; Aoki, S.; Ono, M. Respiratory Health Associated with Exposure to Automobile Exhaust. I. Results of Cross-sectional Studies in 1979, 1982, and 1983. *Arch. Environ. Health Int. J.* **1993**, *48*, 53–58. [CrossRef] [PubMed]
4. Riediker, M.; Cascio, W.E.; Griggs, T.R.; Herbst, M.C.; Bromberg, P.A.; Neas, L.; Williams, R.W.; Devlin, R.B. Particulate Matter Exposure in Cars Is Associated with Cardiovascular Effects in Healthy Young Men. *Am. J. Respir. Crit. Care Med.* **2004**, *169*, 934–940. [CrossRef] [PubMed]
5. Finn, D.; Clawson, K.L.; Carter, R.G.; Rich, J.D.; Eckman, R.M.; Perry, S.G.; Isakov, V.; Heist, D.K. Tracer studies to characterize the effects of roadside noise barriers on near-road pollutant dispersion under varying atmospheric stability conditions⋆. *Atmospheric Environ.* **2010**, *44*, 204–214. [CrossRef]
6. Ning, Z.; Hudda, N.; Daher, N.; Kam, W.; Herner, J.; Kozawa, K.; Mara, S.; Sioutas, C. Impact of roadside noise barriers on particle size distributions and pollutants concentrations near freeways. *Atmospheric Environ.* **2010**, *44*, 3118–3127. [CrossRef]
7. Clawson, K.L.; Eckman, R.M.; Johnson, R.C.; Carter, R.G.; Finn, D.; Rich, J.D.; Hukari, N.F.; Strong, T.; Beard, S.A.; Reese, B.R. *Near Roadway Tracer Study*; NOAA Technical Memorandum OAR ARL-260; Air Resources Laboratory: Idaho Falls, ID, USA, 2008.
8. Heist, D.; Perry, S.; Brixey, L. A wind tunnel study of the effect of roadway configurations on the dispersion of traffic-related pollution. *Atmospheric Environ.* **2009**, *43*, 5101–5111. [CrossRef]
9. Hagler, G.S.; Lin, M.-Y.; Khlystov, A.; Baldauf, R.W.; Isakov, V.; Faircloth, J.; Jackson, L.E. Field investigation of roadside vegetative and structural barrier impact on near-road ultrafine particle concentrations under a variety of wind conditions. *Sci. Total. Environ.* **2012**, *419*, 7–15. [CrossRef]
10. Schulte, N.; Snyder, M.; Isakov, V.; Heist, D.; Venkatram, A. Effects of solid barriers on dispersion of roadway emissions. *Atmospheric Environ.* **2014**, *97*, 286–295. [CrossRef]
11. Baldauf, R.W.; Isakov, V.; Deshmukh, P.; Venkatram, A.; Yang, B.; Zhang, K.M. Influence of solid noise barriers on near-road and on-road air quality. *Atmospheric Environ.* **2016**, *129*, 265–276. [CrossRef]
12. Venkatram, A.; Heist, D.K.; Perry, S.G.; Brouwer, L. Dispersion at the edges of near road noise barriers. *Atmospheric Pollut. Res.* **2020**. [CrossRef]
13. Steffens, J.T.; Wang, Y.J.; Zhang, K.M. Exploration of effects of a vegetation barrier on particle size distributions in a near-road environment. *Atmospheric Environ.* **2012**, *50*, 120–128. [CrossRef]
14. Steffens, J.T.; Heist, D.K.; Perry, S.G.; Zhang, K.M. Modeling the effects of a solid barrier on pollutant dispersion under various atmospheric stability conditions. *Atmospheric Environ.* **2013**, *69*, 76–85. [CrossRef]
15. Adair, D.; Jaeger, M. Evaluation of model for air pollution in the vicinity of roadside solid barriers. *Energy Environ. Eng.* **2014**, *2*, 145–152.
16. Jeong, S.J. A CFD Study of Roadside Barrier Impact on the Dispersion of Road Air Pollution. *Asian J. Atmospheric Environ.* **2015**, *9*, 22–30. [CrossRef]
17. Morakinyo, T.E.; Lam, Y.F. Simulation study of dispersion and removal of particulate matter from traffic by road-side vegetation barrier. *Environ. Sci. Pollut. Res.* **2015**, *23*, 6709–6722. [CrossRef] [PubMed]
18. Tong, Z.; Baldauf, R.W.; Isakov, V.; Deshmukh, P.; Zhang, K.M. Roadside vegetation barrier designs to mitigate near-road air pollution impacts. *Sci. Total. Environ.* **2016**, *541*, 920–927. [CrossRef]

19. Ranasinghe, D.; Lee, E.S.; Zhu, Y.; Frausto-Vicencio, I.; Choi, W.; Sun, W.; Mara, S.; Seibt, U.; Paulson, S.E. Effectiveness of vegetation and sound wall-vegetation combination barriers on pollution dispersion from freeways under early morning conditions. *Sci. Total. Environ.* **2019**, *658*, 1549–1558. [CrossRef] [PubMed]
20. Wang, S.; Wang, X. Modeling and analysis of highway emission dispersion due to noise barrier and automobile wake effects. *Atmospheric Pollut. Res.* **2021**, *12*, 67–75. [CrossRef]
21. Reiminger, N.; Jurado, X.; Vazquez, J.; Wemmert, C.; Blond, N.; Dufresne, M.; Wertel, J. Effects of wind speed and atmospheric stability on the air pollution reduction rate induced by noise barriers. *J. Wind. Eng. Ind. Aerodyn.* **2020**, *200*, 104160. [CrossRef]
22. Huertas, J.I.; Sánchez, D.F.P. An experimental and numerical study of air pollution near unpaved roads. *Air Qual. Atmosphere Health* **2019**, *12*, 471–489. [CrossRef]
23. Huertas, J.I.; Martínez, D.S.; Prato, D.F. Effects of the atmospheric stability conditions on the dispersion of pollutants over flat areas. *Scientific Rep. Nat.* **2021**. (Currently under review).
24. Busini, V.; Rota, R. Influence of the shape of mitigation barriers on heavy gas dispersion. *J. Loss Prev. Process. Ind.* **2014**, *29*, 13–21. [CrossRef]
25. Gerdroodbary, M.B.; Mokhtari, M.; Bishehsari, S.; Fallah, K. Mitigation of Ammonia Dispersion with Mesh Barrier under Various Atmospheric Stability Conditions. *Asian J. Atmospheric Environ.* **2016**, *10*, 125–136. [CrossRef]
26. Franke, J.; Hellsten, A.; Schlünzen, H.; Carissimo, B. *Best Practice Guideline for the CFD Simulation of Flows in the Urban Environment: COST Action 732 Quality Assurance and Improvement of Microscale Meteorological Models*; Meteorological Institute: Hamburg, Germany, 2007.
27. NZ Transport Agency. *NZTA State Highway Noise*; NZ Transport Agency: Wellington, New Zealand, 2010.
28. U.S. Department of Transportation. *Highway Traffic Noise: Analysis and Abatement Guidance*; U.S. Department of Transportation: Washington, DC, USA, 2011.
29. State of Queensland, Department of Transport and Main Roads. *Transport Noise Management*; State of Queensland, Department of Transport and Main Roads: Queensland, Australia, 2013.
30. Arya, S. *Introduction to Micrometeorology*; Academic Press: Cambridge, MA, USA, 1988.
31. Stull, R. *The Atmospheric Boundary Layer. An Introduction to Boundary Layer Meteorology*; Springer: Amsterdam, The Netherlands, 2005; pp. 375–418.
32. Stull, R. *Practical Meteorology: An Algebra-Based Survey of Atmospheric Science*; University of British Columbia: Vancouver, BC, Canada, 2016; pp. 797–801.
33. Blocken, B.B.; Gualtieri, C. Ten iterative steps for model development and evaluation applied to Computational Fluid Dynamics for Environmental Fluid Mechanics. *Environ. Model. Softw.* **2012**, *33*, 1–22. [CrossRef]
34. Obukhov, A.M. Turbulence in an atmosphere with a non-uniform temperature. *Boundary-Layer Meteorol.* **1971**, *2*, 7–29. [CrossRef]
35. Zoras, S.; Triantafyllou, A.; Deligiorgi, D. Atmospheric stability and PM10 concentrations at far distance from elevated point sources in complex terrain: Worst-case episode study. *J. Environ. Manag.* **2006**, *80*, 295–302. [CrossRef] [PubMed]
36. Pieterse, J.; Harms, T. CFD investigation of the atmospheric boundary layer under different thermal stability conditions. *J. Wind. Eng. Ind. Aerodyn.* **2013**, *121*, 82–97. [CrossRef]
37. Xia, Q.; Niu, J.; Liu, X. Dispersion of air pollutants around buildings: A review of past studies and their methodolo-gies. *Indoor Built Environ.* **2014**, *23*, 201–224. [CrossRef]
38. Alinot, C.; Masson, C. k-ϵ Model for the Atmospheric Boundary Layer Under Various Thermal Stratifications. *J. Sol. Energy Eng.* **2005**, *127*, 438–443. [CrossRef]
39. Wang, Y.J.; Zhang, K.M. Modeling Near-Road Air Quality Using a Computational Fluid Dynamics Model, CFD-VIT-RIT. *Environ. Sci. Technol.* **2009**, *43*, 7778–7783. [CrossRef] [PubMed]
40. ANSYS. *Theory Guide*; ANSYS, Inc.: Canonsburg, PA, USA, 2012.
41. Walvoord, M.A.; Andraski, B.J.; Green, C.T.; Stonestrom, D.A.; Striegl, R.G. Field-Scale Sulfur Hexafluoride Tracer Experiment to Understand Long Distance Gas Transport in the Deep Unsaturated Zone. *Vadose Zone J.* **2014**, *13*, 1–10. [CrossRef]
42. Blocken, B.; Stathopoulos, T.; Carmeliet, J. CFD simulation of the atmospheric boundary layer: Wall function problems. *Atmospheric Environ.* **2007**, *41*, 238–252. [CrossRef]
43. ANSYS. *User Guide*; ANSYS, Inc.: Canonsburg, PA, USA, 2012.
44. Rüedi, I. *WMO Guide to Meteorological Instruments and Methods of Observation: WMO-8 Part I: Measurement of Meteorological Variables, Chapter 1*; World Meteorological Organization: Geneva, Switzerland, 2006.